ACCOUNTS of chemical research

Article

pubs.acs.org/accounts

Electrochemical Liquid–Liquid–Solid (ec-LLS) Crystal Growth: A Low-Temperature Strategy for Covalent Semiconductor Crystal Growth

Eli Fahrenkrug[†] and Stephen Maldonado*[,†,‡]

[†]Department of Chemistry and [‡]Program in Applied Physics, University of Michigan, 930 North University Avenue, Ann Arbor, Michigan 48109-1055, United States

CONSPECTUS: This Account describes a new electrochemical synthetic strategy for direct growth of crystalline covalent group IV and III–V semiconductor materials at or near ambient temperature conditions. This strategy, which we call "electrochemical liquid–liquid–solid" (ec-LLS) crystal growth, marries the semiconductor solvation properties of liquid metal melts with the utility and simplicity of conventional electrodeposition. A low-temperature liquid metal (i.e., Hg, Ga, or alloy thereof) acts simultaneously as the source of electrons for the heterogeneous reduction of oxidized semiconductor precursors dissolved in an electrolyte as well as the solvent for dissolution of the zero-valent semiconductor. Supersaturation of the semiconductor in the liquid metal triggers eventual crystal nucleation and growth. In this way, the liquid electrolyte–liquid metal–solid crystal phase boundary strongly influences crystal growth.

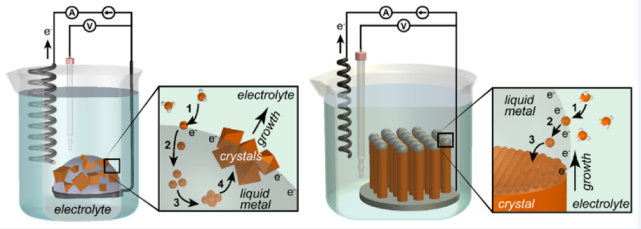

As a synthetic strategy, ec-LLS has several intrinsic features that are attractive for preparing covalent semiconductor crystals. First, ec-LLS does not require high temperatures, toxic precursors, or high-energy-density semiconductor reagents. This largely simplifies equipment complexity and expense. In practice, ec-LLS can be performed with only a beaker filled with electrolyte and an electrical circuit capable of supplying a defined current (e.g., a battery in series with a resistor). By this same token, ec-LLS is compatible with thermally and chemically sensitive substrates (e.g., plastics) that cannot be used as deposition substrates in conventional syntheses of covalent semiconductors. Second, ec-LLS affords control over a host of crystal shapes and sizes through simple changes in common experimental parameters. As described in detail herein, large and small semiconductor crystals can be grown both homogeneously within a liquid metal electrode and heterogeneously at the interface of a liquid metal electrode and a seed substrate, depending on the particular details chosen for ec-LLS. Third, the rate of introduction of zero-valent materials into the liquid metal is precisely gated with a high degree of resolution by the applied potential/current.

The intent of this Account is to summarize the key elements of ec-LLS identified to date, first contextualizing this method with respect to other semiconductor crystal growth methods and then highlighting some unique capabilities of ec-LLS. Specifically, we detail ec-LLS as a platform to prepare Ge and Si crystals from bulk- (~1 cm^3), micro- (~10^{-10} cm^3), and nano-sized (~10^{-16} cm^3) liquid metal electrodes in common solvents at low temperature. In addition, we describe our successes in the preparation of more compositionally complex binary covalent III–V semiconductors.

I. SEMICONDUCTOR CRYSTAL GROWTH

Crystalline covalent semiconductors are ubiquitous in society as backbones of many communications, energy, and sensing technologies.[1−4] Current industrial manufacturing methods for groups IV and III–V semiconductors are energy- and resource-intensive,[5−7] since no group IV or III–V semiconductor occurs naturally on this planet. Instead, they must be prepared from heavily oxidized ores and oxides found in nature.

Approaches for the preparation of covalent semiconductor materials can be broadly classified as bulk or thin-film methods. Methods that produce bulk macroscopic semiconductors generally first involve steps to reduce raw oxides to elemental semiconductors. The raw zero-valent materials are then recrystallized in hot (T > 1400 °C for Si) melts of the target semiconductor using Czochralski, Bridgman, or float-zone techniques. These multistep processes can yield large (>1 cm^3), high-quality single crystals but are unsuitable for thin films.[8] A variation of this concept is liquid-phase epitaxy (LPE). In LPE, a previously prepared raw semiconductor powder is first dissolved into a liquid metal solvent at an elevated temperature. The temperature of the metal melt is then lowered to attain supersaturation and promote crystal nucleation and growth (Figure 1a).[9] LPE is naturally suited to the preparation of semiconductor films with few defects, low levels of impurities, and large crystalline domains.[9] However, LPE is not actively used in industrial semiconductor manufacturing because thin films cannot be deposited with sufficient precision and LPE reactor designs are cumbersome.[9,10] Liquid-phase electroepitaxy (LPEE) is a variation of LPE in which a large, non-Faradaic electrical current is passed through the metal melt during crystal growth. The current is large (10^1 A cm^{-2}) to induce local Joule heating and Peltier

Received: March 30, 2015
Published: July 1, 2015

DOI: 10.1021/acs.accounts.5b00158
Acc. Chem. Res. 2015, 48, 1881−1890

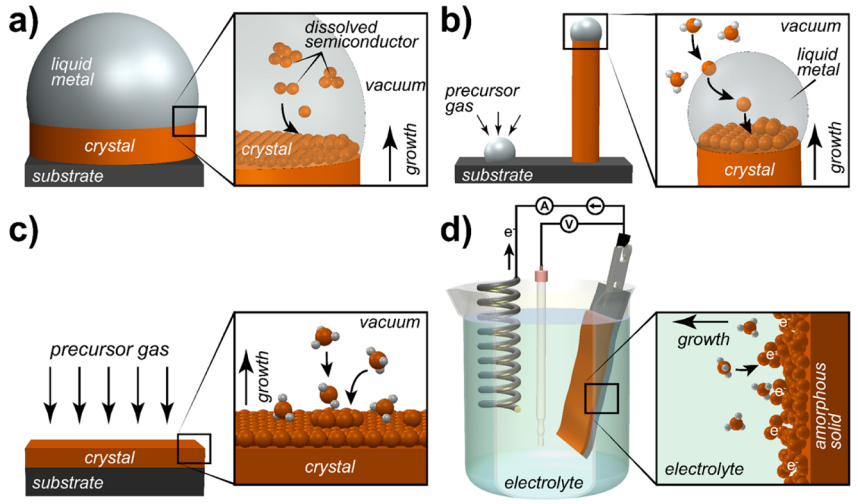

Figure 1. Schematic representations of select semiconductor crystal growth strategies, including (a) liquid-phase epitaxy, (b) vapor−liquid−solid or solution−liquid−solid growth, (c) vapor-phase deposition, and (d) conventional electrodeposition. Not drawn to scale.

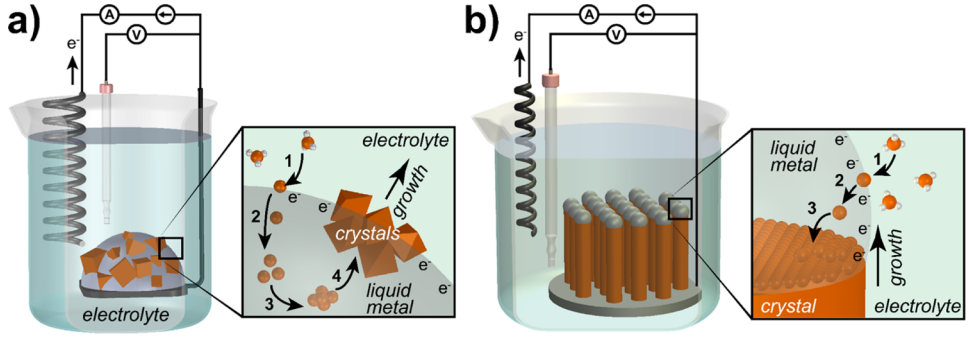

Figure 2. Schematic depictions of the experimental setup and steps (insets) of ec-LLS semiconductor crystal growth from (a) bulk and (b) nano/microscale liquid metal-droplet electrodes. ec-LLS proceeds through (1) electrochemical reduction of a dissolved ionic precursor in the electrolyte solution followed by (2) dissolution of the zero-valent semiconductor into the liquid metal electrode. In (a), steps (3) and (4) highlight homogeneous nucleation and subsequent crystal growth, respectively. In (b), step (3) depicts heterogeneous nucleation at a crystal seed interface and subsequent layer-by-layer crystal growth. Not drawn to scale.

cooling at the respective electrodes, enhancing the driving force for nucleation.[11]

For the growth of micro- and nanoscale crystals, vapor−liquid−solid (VLS) and solution−liquid−solid (SLS) methods are similar to LPE but employ much smaller diameter (10^{-9} − 10^{-6} m) liquid metals (Figure 1b). VLS specifically involves the decomposition of gas-phase reactants in a hot reactor (typically) under vacuum to introduce zero-valent semiconductors into the molten liquid metal. SLS separately requires the decomposition of molecular reactants dissolved in a hot liquid solvent free of any water or O_2. VLS and SLS have proven useful for the synthesis and study of micro- and nanocrystalline materials but also share some intrinsic drawbacks as manufacturing strategies.[12−14] First, high temperatures and/or low pressures are required to drive the thermal decomposition of the precursors to their zero-valent forms.[12,13,15,16] Second, both techniques employ heavily refined and expensive semiconductor precursor compounds that are often toxic and are themselves resource-intensive to synthesize, handle, and store.[16,17] Third, the combination of high temperature, low pressure, and noxious precursors imposes serious constraints on the compatibility of deposition substrates,[18,19] metal catalyst identity,[20] and high-throughput reactor designs that do not introduce substantial material inhomogeneity.[12−14]

The preparation of thin semiconductor films does not usually involve melts. Molecular beam epitaxy (MBE) and metal organic chemical vapor deposition (MOCVD) are gas-phase deposition strategies based on the reaction of atomic or molecular precursors impinging on a hot deposition substrate (Figure 1c). Compositionally complex crystalline semiconductor thin films can be produced with excellent electrical properties and thickness control. However, both techniques require elaborate and expensive vacuum-based reactors,[5,8,21] vapor-phase precursors that are heavily processed/refined/energy-rich,[5] and high process temperatures (T > 600 °C) to promote good crystallinity.[5,21]

In contrast, electrodeposition has long been explored as a possible alternative route for semiconductor films. The principal draw is the comparatively simple instrumentation/setup and the possibility of deposition at low temperatures.[22,23] "Conventional" electrodeposition is defined by solid electrodes immersed in an electrolyte bath with dissolved oxidized precursors. A negative bias applied to the solid cathode drives the heterogeneous electroreduction to the zero-valent state (Figure 1d). Despite its simplicity, "conventional" electrodeposition has three major drawbacks. First, low-temperature (T < 500 °C) electrodeposition always produces amorphous solids with high impurity content (e.g., solvent and supporting electrolyte). The poor purity/crystallinity of these films

DOI: 10.1021/acs.accounts.5b00158
Acc. Chem. Res. 2015, 48, 1881−1890

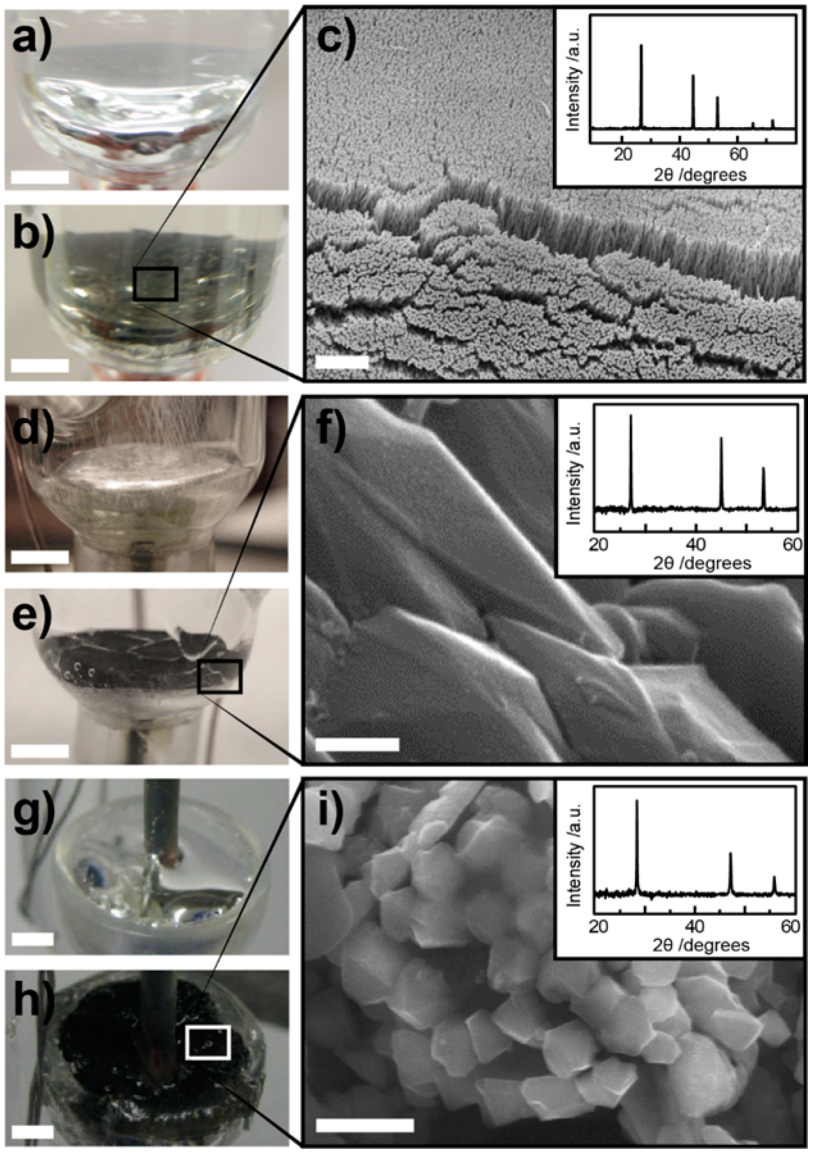

Figure 3. (a, b) Optical photographs of a bulk Hg(l) electrode (a) before and (b) after room-temperature Ge ec-LLS at −2.7 V vs Ag/AgCl from an aqueous electrolyte containing 0.05 M GeO_2 and 0.01 M $Na_2B_4O_7$. (c) Electron micrograph and (inset) powder X-ray diffraction pattern collected from the as-deposited material shown in (b). (d, e) Optical photographs of a bulk Ga(l) electrode (d) before and (e) after room-temperature Ge ec-LLS at −1.6 V vs Ag/AgCl from the same aqueous electrolyte as used in (b). (f) Tilted electron micrograph and (inset) powder X-ray diffractogram of crystals produced in (e). (g, h) Optical photographs of a bulk Ga(l) electrode (g) before and (h) after Si ec-LLS at 20 mA cm^{-2} for 2 h at 100 °C from a propylene carbonate electrolyte with 0.5 M $SiCl_4$ and 0.2 M TBACl. (i) Scanning electron micrograph and (inset) powder X-ray diffraction pattern of crystals produced in (h). Scales are (a, b, d, e, g, h) 2 mm and (c, f, i) 1 μm. Panels (a−c) are adapted from ref 33. Copyright 2011 American Chemical Society. Panels (g−i) are adapted from ref 35. Copyright 2013 American Chemical Society.

necessitates thermal processing, negating any cost advantage.[24−26] Second, high-temperature electrodeposition requires solvents such as the aforementioned melts and the use of sacrificial anodes.[27−29] Third, electrodeposition of compositionally complex (e.g., binary, ternary, quaternary) semiconductors requires simultaneous co-electrodeposition of multiple species. Doing so with sufficient precision to effect a precise stoichiometry throughout the entirety of the film is extremely challenging.[26,30] Electrochemical atomic layer epitaxy (ECALE)[31,32] stands apart in this regard, as stoichiometric and highly ordered II−VI films can be made via ECALE. However, although ECALE methods are apt for ionic semiconductors, ECALE of covalent groups IV and III−V semiconductor films is extremely challenging.

II. EC-LLS

The hallmark of ec-LLS is a liquid metal acting both as an electron source for the heterogeneous reduction of oxidized precursors and as a separate phase for solvating the deposit. In certain cases, the liquid metal can also act as a reagent. Two specific variations of ec-LLS will be the focus of this Account and are shown in Figure 2. In both types, ec-LLS begins with the application of an electrochemical potential to a liquid metal electrode, providing the driving force for reduction of the dissolved precursor to the zero-valent state (Figure 2, step 1). Electrical connection to the liquid metals is made using a small Pt wire in macroscale electrodes[33−35] and directly through a conductive support in the case of micro- and nanoscale liquid metals.[36−38] Continued electrochemical reduction of the

DOI: 10.1021/acs.accounts.5b00158
Acc. Chem. Res. 2015, 48, 1881−1890

Table 1. Physical Properties of Select Liquid Metals

	Hg	Ga	In	ref
melting point/°C	−38.3	29.8	156.6	39
density[a]/g cm^{-3}	13.53	6.09	7.02	39
viscosity[a]/mPa s	1.6	1.5	1.8	40
surface tension[a]/N m^{-1}	0.47	0.71	0.57	41
Si solubility[b]/atom %	<4 × 10^{-11}	1.1 × 10^{-7}	1.9 × 10^{-13}	42, 43
Ge solubility[b]/atom %	3 × 10^{-7}	4.5 × 10^{-3}	8.6 × 10^{-5}	42, 44
exchange current density[c]/A cm^{-2}	10$^{-12.66}$	10$^{-9.92}$	10$^{-10.83}$	45

[a]Measured at the melting point. [b]Extrapolated to 30 °C. [c]Measured with 0.1 M $HClO_4$ in water, H^+/H_2 couple, 30 °C.

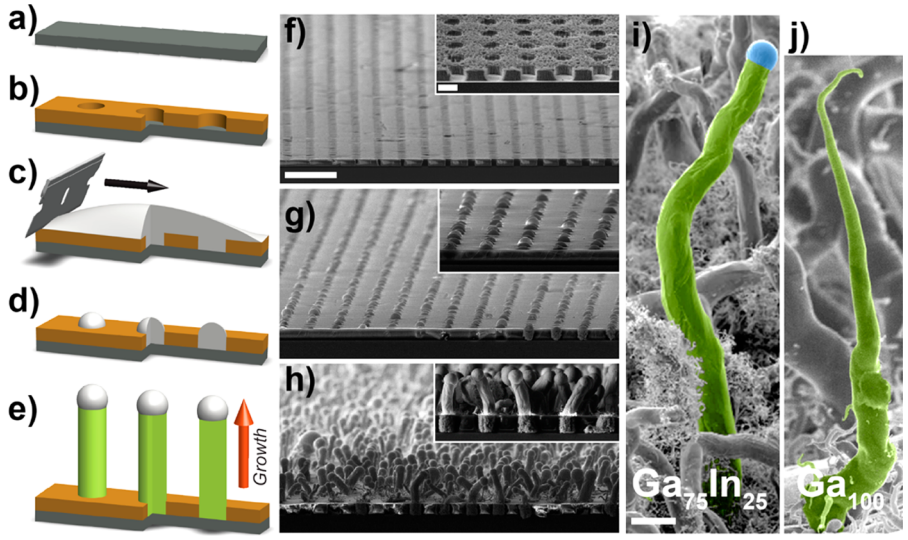

Figure 4. (a–e) Schematic illustration of the sequence for preparing arrays of liquid metal microelectrodes. A flat conductive support (a) is photolithographically patterned (b), leaving through-holes of defined size and pitch. (c) Bulk liquid metal is doctor-bladed repeatedly over the surface to fill the exposed holes. (d) Excess liquid metal is removed, leaving ordered arrays of discrete liquid metal microelectrodes. (e) These arrays of liquid metal microdroplets are active for ec-LLS microwire growth. (f–h) Tilted scanning electron micrographs of the steps depicted in (b), (d), and (e), respectively. Scale bar = 50 μm. The insets show high-magnification views. Scale bar = 10 μm. (i, j) Tilted scanning electron micrographs of Ge microwires grown from (i) EGaIn (75% Ga, 25% In by weight) and (j) pure Ga electrodes following ec-LLS growth at T = 80 °C for 120 min. Scale bar = 10 μm. Adapted from ref 36. Copyright 2015 American Chemical Society.

precursor establishes a concentration gradient between the surface and interior of the liquid metal, which drives dissolution of the semiconductor into the bulk of the liquid metal solution (step 2). When the concentration surpasses the equilibrium solubility of the semiconductor in the metal solution, crystal nucleation (step 3) and growth (step 4) ensue. Removal of the electrochemical driving force results in immediate cessation of ec-LLS.

ec-LLS is a true hybrid, combining the best features of all the methods described in Figure 1. As in conventional electrodeposition, raw, oxidized precursors are used as inputs. In this sense, ec-LLS is a *synthetic* method and thus stands apart from the melt recrystallizations described above that require separate prior steps to form the reduced semiconductor. However, unlike conventional electrodeposition, ec-LLS products are fully crystalline, even at low temperatures. As in melt growths, the liquid metals in ec-LLS solvate fully reduced semiconductors and facilitate crystal growth. Accordingly, our group has demonstrated the direct production of crystalline Ge-, Si-, and Ga-based III–V semiconductors and In-containing III–V semiconductors under purely benchtop conditions.

III. EC-LLS SYNTHESIS OF CRYSTALLINE GROUP IV SEMICONDUCTORS

The first demonstration of the ec-LLS process involved the electrodeposition of Ge on macroscopic (~1 cm^3) liquid Hg electrodes immersed in aqueous solutions containing GeO_2 (eq 1):

$$HGeO_3^-(aq) + 4e^- + 2H_2O(l) \rightarrow Ge(s) + 5OH^-(aq) \quad (1)$$

The optical images in Figure 3a,b collected before and after ec-LLS, respectively, show a macroscopically thick black material emerging from the surface of the liquid metal within minutes. Powder X-ray diffraction (Figure 3c, inset), transmission electron microscopy (TEM), and Raman analyses highlighted the crystallinity of as-deposited Ge^0.[33] Similar observations were made when Ga was substituted for Hg (Figure 3e,f). The total quantity of Ge was a function of the total electrodeposition time for both Hg and Ga electrodes, and the growth ceased upon removal of the applied potential/current. Control experiments with solid (frozen) Ga electrodes yielded substantially less Ge^0 and an absence of detectable crystallinity by diffraction.

The microstructure and morphology of Ge produced by ec-LLS depended strongly on the type of liquid metal electrode.

DOI: 10.1021/acs.accounts.5b00158
Acc. Chem. Res. 2015, 48, 1881–1890

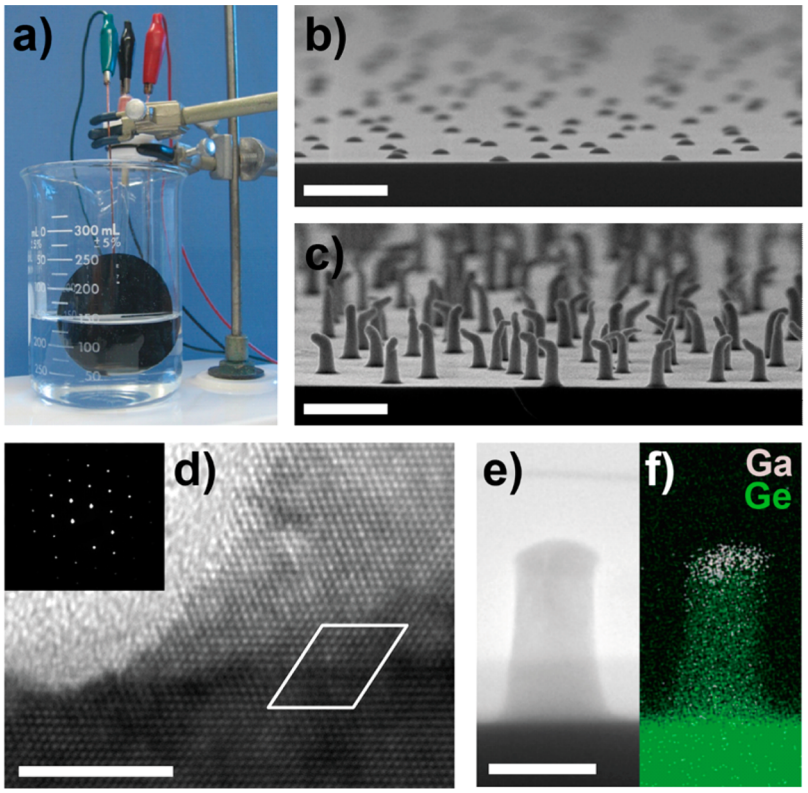

Figure 5. (a) Photograph depicting the benchtop experimental setup used for wafer-scale ec-LLS of Ge nanowire films. (b, c) Cross-sectional scanning electron micrographs of a Ge(111) substrate decorated with discrete liquid Ga nanodroplets (b) before and (c) after 60 s ec-LLS process with the setup in (a). Scale bars = 500 nm. (d) Cross-sectional HR-TEM view of the interface between the base of a Ge nanowire prepared by ec-LLS and the n^+-Ge(111) substrate viewed along the [1$\bar{1}$0] zone axis. Scale bar = 5 nm. Inset: SAED pattern collected over the nanowire−substrate interface. (e) Cross-sectional HRTEM view of an as-prepared single Ge nanowire on a wafer substrate produced after 30 s of ec-LLS. Scale bar = 100 nm. (f) Energy-dispersive X-ray spectroscopic elemental map of the structure in (e). Adapted from ref 37. Copyright 2014 American Chemical Society.

Figure 3c shows the nanostructured and filamentous morphology of Ge crystals produced on bulk Hg(l) electrodes at E_{app} = −2.7 V vs Ag/AgCl. Extensive electron microscopy and diffraction studies indicated that the crystalline domain size was on the order of 10^{-8} m. Under comparable ec-LLS conditions with Ga electrodes, we observed a completely different faceted structure with much larger crystalline domains (Figure 3f). X-ray and electron backscatter diffraction studies showed crystalline Ge grain sizes in excess of 10^{-5} m, a 1000-fold increase in size relative to the results with Hg. Table 1 summarizes some known physical properties of metals with low melting points.[39−45] The respective solubilities of Ge in Hg and Ga differ considerably at room temperature. From classical nucleation theory, the critical nucleation size of a growing crystal is a function of the solubility.[46] With the assumption that large initial nuclei translate into larger resultant crystal grains, the observations in Figure 3 are in accord with the respective Ge solubilities of Hg and Ga.

Crystalline Si can also be prepared directly through ec-LLS.[35] Figure 3g,h shows images taken before and after the ec-LLS growth of Si films on bulk Ga(l) at 80 °C by electrochemical reduction of $SiCl_4$ dissolved in propylene carbonate through the electrochemical half-reaction shown in eq 2:

$$SiCl_4(l) + 4e^- \rightarrow Si(s) + 4Cl^- \quad (2)$$

Powder X-ray diffraction (Figure 3i, inset) verified separate Raman and electron micrographs showing that the as-prepared Si was fully crystalline. This feat bested the previous temperature for electrodeposition of crystalline Si by roughly 650 °C.[28] The faceted particles in the electron micrographs in Figure 3i were consistent with Si grain sizes in excess of 5 × 10^{-7} m, more than 10 times smaller than the mean grain size for Ge crystals prepared with Ga at the same temperature. A separate study of Si electrodeposition in molten-salt electrolytes by the Bard group reported observations consistent with an ec-LLS mechanism at T = 850 °C,[47] illustrating the large scope of electrode/electrolyte systems for the ec-LLS strategy that have yet to be explored.

One particularly attractive feature of ec-LLS is the ability to control the crystal size and shape by modulating the size of the liquid metal electrode. Nano- and microscale group IV semiconductor crystals can be prepared with liquid metal electrodes of comparable size. To demonstrate this concept, a strategy to prepare liquid metal microdroplets was developed.[36] Conventional photolithography was combined with simple doctor blading to create large-area arrays (>1 cm^2) of discrete liquid metal microelectrodes. Figure 4a−g shows the general premise and subsequent application in ec-LLS. The resultant materials produced in this fashion were crystalline Ge microwires. Scanning electron micrographs (Figure 4h, inset) clearly showed that the liquid metal microdroplet remained affixed to the tip of each resultant Ge microwire produced by ec-LLS, indicating that the initial nucleation event occurred at the underlying liquid metal−substrate interface. A tip-based ec-LLS growth mechanism is analogous to VLS and SLS crystal

DOI: 10.1021/acs.accounts.5b00158
Acc. Chem. Res. 2015, 48, 1881−1890

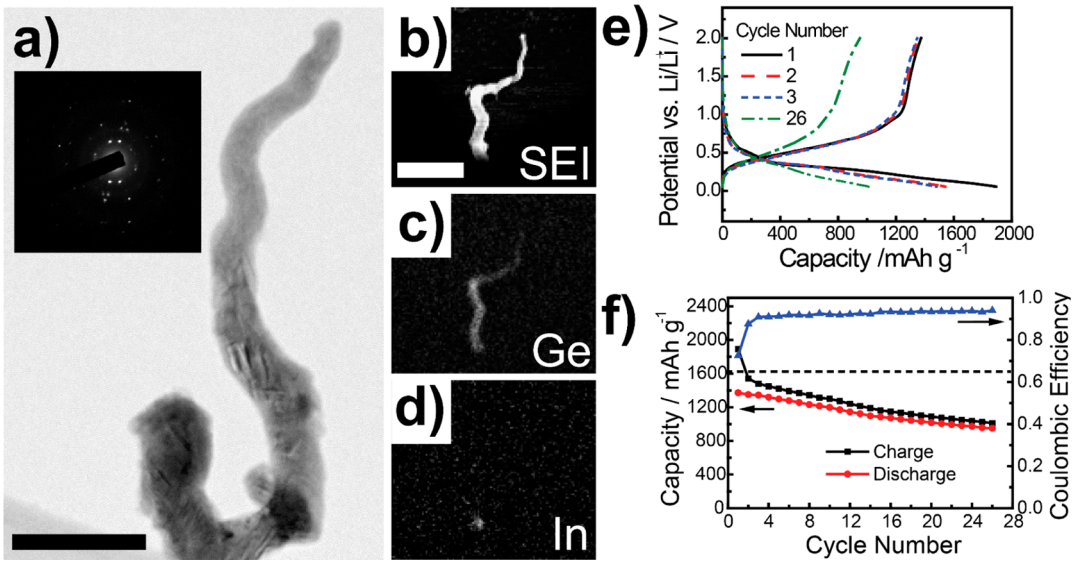

Figure 6. (a) TEM image of an individual Ge nanowire electrodeposited at −2.0 V vs Ag/AgCl for 10 min at room temperature from 0.05 M GeO_2 and 0.01 M $Na_2B_4O_7$ dissolved in water. Scale bar = 50 nm. (b) Secondary electron image (SEI) of an individual Ge nanowire electrodeposited at −2.0 V vs Ag/AgCl for 10 min. Scale bar = 500 nm. (c, d) Energy-dispersive spectroscopic elemental mapping of the same area as in (b) with the detector channel for (c) the Lα line of Ge and (d) the M line of In. (e) First, second, third, and 26th charge−discharge curves for a Li^+ anode recorded at a rate of 1 C using an as-prepared Ge nanowire film. (f) Galvanostatic Li^+ charge (black squares) and discharge (red circles) cycling at a rate of 1 C using an as-prepared Ge nanowire film. The Coulombic efficiencies for individual charge−discharge cycles are indicated on the right axis (blue triangles). Adapted from ref 38. Copyright 2012 American Chemical Society.

growth schemes.[12,13,16] The important distinction for ec-LLS is the electrochemical "cracking" of the precursor.

The method of doctor-blading liquid metals into polymer templates afforded straightforward tests of the ec-LLS process. First, to test whether microwire growth by ec-LLS can be performed on any type of conductive support, ec-LLS was performed with liquid metal microdroplets resting on Si wafers, Cu foil, Ti foil, stainless steel, indium tin oxide, and PEDOT:PSS polymer films.[36] Every substrate supported ec-LLS of Ge microwires. Electrodeposition of crystalline inorganic semiconductors on organic substrates is particularly attractive from the perspective of device fabrication, representing a unique advantage of ec-LLS. Second, to compare the influence of the type of liquid metal, different liquid metals were doctor-bladed into the templates. Figure 4i,j shows scanning electron micrographs of two Ge microwires grown from Ga−In eutectic (EGaIn) and Ga microdroplets under otherwise identical ec-LLS conditions. Both liquid metals facilitated heterogeneous growth of Ge microwires by ec-LLS, but the resultant morphology was particularly sensitive to the electrode composition. Ge microwires produced with Ga microdroplets exhibited a smooth (unfaceted) surface and significant taper along the axial direction, with a diameter reduction from 10.2 to 0.8 μm over a total length of 120.5 μm (cone angle = 2.23°). After 45 min of growth, the liquid metal cap was completely absent, and ec-LLS growth terminated. In contrast, Ge microwires electrodeposited with EGaIn microdroplets were faceted and much less tapered, with a diameter decrease of 10.1 to 6.5 μm over a total length of 124.9 μm (cone angle = 0.83°). The specific microscopic origin of these differences has yet to be identified conclusively. However, since heterogeneous crystal growth models show that the surface tension at a three-phase interface (in this case between the liquid electrolyte, liquid metal, and solid semiconductor crystal) strongly influences the crystal growth,[48] the ec-LLS observations suggest that changes in surface properties of the liquid metal may be important.

Crystalline semiconductor nanowires can be obtained with liquid metal nanodroplets. Figure 5 demonstrates the concept for ec-LLS of Ge nanowires.[37] Figure 5a−c shows that a film of Ga nanodroplets on a single-crystalline wafer could be used as a massively parallel ultramicroelectrode array for ec-LLS. After an ec-LLS experiment lasting just 60 s, each individual Ga nanodroplet acted as a site for the electrodeposition of a single Ge nanowire. Separate studies showed a linear correlation between the nanodroplet and nanowire sizes.[49] Transmission and scanning electron microscopy indicated that the wires grew collinear to the [111] direction of the wafer substrate, suggestive of an epitaxial interface. The electron micrographs and selected area electron diffraction (SAED) pattern of the substrate−nanowire interface in Figure 5d confirmed that the nanowire was an extension of the underlying crystalline substrate (i.e., epitaxy). In fact, we showed both homoepitaxy and heteroepitaxy in ec-LLS of Ge nanowires.[37] In these experiments, the liquid Ga nanodroplets were always observed on the tip of the Ge nanowire. For longer ec-LLS nanowire experiments, stacking faults were observed that caused kinking.[37] Notably, all of the nanowires across a given film showed kinking at essentially the same position (Figure 5c), implying that the stacking faults formed consistently and simultaneously for each nanowire. A consequence of the stacking faults was an abrupt change in growth direction within the [111] family. Although such defects are undesirable in an absolute sense, the uniformity of this observation without disruption of the continuity of crystallinity suggests that further refinements in ec-LLS deposition parameters could yield large-area films of single-crystalline nanowires with deterministically controlled and uniform properties.

Indium nanoparticles have also been explored for nanowire ec-LLS by our group.[38] Although bulk In is a solid at room temperature, In nanoparticles on Ge show fluid-type behavior

DOI: 10.1021/acs.accounts.5b00158
Acc. Chem. Res. 2015, 48, 1881−1890

at room temperature.[50] For this reason, we evaluated their capacity to facilitate ec-LLS crystal growth. We first prepared In nanoparticles on degenerately doped n-type Si(100) (n^+-Si(100)) wafers via pulse electroplating. As electrodes for ec-LLS, two distinct features were observed for Ge nanowires grown from In nanoparticles. First, these Ge nanowires were highly *polycrystalline*, as evidenced by TEM and corresponding electron diffraction patterns (Figure 6a). Second, the individual In nanoparticle electrodes remained affixed at the base of the Ge nanowire during and after growth (Figure 6b–d), in direct contrast to what had been observed with Ga. This latter observation implied an ec-LLS mechanism that proceeded through crystal nucleation at the In–electrolyte interface, precluding the possibility of any epitaxial relation with the underlying Si substrate. Conversely, the Switzer group separately observed tip-based Ge nanowire ec-LLS growth with In nanoparticle electrodes under slightly different conditions.[51] The specific nucleation mode (i.e., heterogeneous vs homogeneous) and resultant ec-LLS crystal growth mechanism (i.e., root vs tip growth) is clearly sensitive to the substrate identity, volume of liquid metal, and growth temperature, but the specific weighting of each factor merits further quantitative investigation.

Nanowires prepared by ec-LLS with the liquid metal nanodroplets still in contact with the underlying conductive support are desirable for electronic applications. We prepared dense Ge nanowire films with In nanoparticles at their base and then tested their capacity to function as Li^+ battery anodes without further processing. Figure 6e,f shows the charge–discharge curves for Ge nanowire film electrodes prepared by In-based ec-LLS. The major finding was that the cycling activity of these nanowire electrodes was essentially identical to (if not superior to) those previously reported for nanostructured Ge Li^+ battery anodes (Table 2).[52−57] The key distinction was that our materials were prepared *at room temperature in an aqueous solution on the benchtop*.

IV. EC-LLS SYNTHESIS OF CRYSTALLINE GROUP III–V SEMICONDUCTORS

The synthesis of covalent III–V semiconductor crystals is also possible through ec-LLS if the liquid metal also acts as a reactant. Our first attempt to prepare a III–V semiconductor by ec-LLS involved the electrodeposition of As onto a liquid Ga electrode.[34] In an alkaline bath, dissolved As_2O_3 was electroreduced through the electrochemical half-reaction shown in eq 3:

$$HAsO_3^{2-}(aq) + 3e^- + 2H_2O(l) \rightarrow As(s) + 5OH^-(aq) \quad (3)$$

The hypothesis was that when As^0 was formed at the interface, the reaction between As^0 and Ga^0 to form GaAs (eq 4),

$$Ga(l) + As(s) \rightarrow GaAs(s) \quad (4)$$

should be spontaneous even at room temperature (ΔG° = −83.7 kJ mol^{-1}). Since GaAs has some solubility in Ga, these reactions should result in GaAs crystals.

The initial attempts at GaAs ec-LLS were not successful. Despite the fact that electroreduction of dissolved As_2O_3 at Ga electrodes occurred readily at overpotentials as low as 300 mV, the only product was amorphous As. Two critical aspects of this ec-LLS process became apparent through subsequent investigations. First, the surface of the liquid Ga electrode had to be clean of any oxides/hydroxides of gallium that naturally form in air and water. This criterion could be satisfied only at electrochemical potentials negative of the standard reduction potential of Ga_2O_3 to Ga (E° = −1.2 V vs NHE). Second, the flux of As^0 introduced onto the Ga^0 surface had to be sufficiently small to prevent accumulation of excess As. Apparently in this ec-LLS system, the dissolution of As into Ga was rate-limiting. If As^0 deposition was too fast, As clusters accumulated, and the Ga surface was effectively passivated with a thick layer of amorphous As^0. In other words, the rate of the electroreduction step (eq 3) had to be carefully controlled so as not to outpace the alloying step (eq 4). One simple way to satisfy this requirement was to decrease the formal concentration of As_2O_3 in the electrolyte, thereby ensuring that the density of As^0 nuclei at the interface would be small. At As_2O_3 concentrations below 1 mM, the electroreduction of As_2O_3 yielded polycrystalline films of GaAs (Figure 7a). The grain size of these films was small (Figure 7b) but was strongly sensitive to temperature. Figure 7c shows Raman spectra collected from GaAs films prepared at different As_2O_3 concentrations with otherwise identical ec-LLS conditions. At high concentrations (>10 mM), only the Raman signal for amorphous As was obtained. At the lowest concentration (<0.1 mM), only pure crystalline GaAs phase was observed. For GaAs produced from 0.1 mM As_2O_3 electrolyte, the film thickness could be tracked optically as a color change. The film color was consistent with the thickness change in the GaAs film, which increased as a function of deposition time. After 120 min of ec-LLS, GaAs films were on the order of 150 nm thick.[34] We tested this mode of ec-LLS for InAs, substituting In as the cathode material in eq 4. Elemental As was again slowly electrodeposited on the In metal surface through eq 3 to effect crystalline InAs films.[58] Aside from the conductive and electrochemically inert nature of the electrolytes used here, these results collectively implicate the precursor concentration as a critical component for ec-LLS electrolyte formulation. Separately, the precursor should be chosen so the reduction potential is sufficiently negative to reduce surface oxides but not so negative that solvent electrolysis presides over precursor reduction. To date, these principles have been applied to ec-LLS of polycrystalline III–V semiconductor films composed of Ga, In, As, and Sb.

Table 2. Reported Discharge Capacities for Ge Li^+ Insertion Anodes[a]

morphology	capacity/ mA h g^{-1}	notes	refs
bulk	≪100	obtained at C/4 after seven cycles	52
thin film	600	evaporated under vacuum	52
nanoparticles	1460	prepared from $GeCl_4$ in dimethoxyethane, dried at 200 °C, butyl-capped	53
nanotubes	765	prepared at 700 °C with Sb, coated with amorphous carbon	54
nanoporous film	1415	prepared from $GeCl_4$, annealed at 800 °C, coated with amorphous carbon	55
nanowires	597	prepared from GeH_4 via VLS at 520 °C, annealed at 320 °C	56
nanostructured film	1004	obtained at C/0.9, prepared from e-beam evaporation and ion beam modification	57
nanowires	973	ec-LLS Ge nanowires from GeO_2 at room temperature	38

[a]Reported at 1 C unless noted otherwise.

DOI: 10.1021/acs.accounts.5b00158
Acc. Chem. Res. 2015, 48, 1881−1890

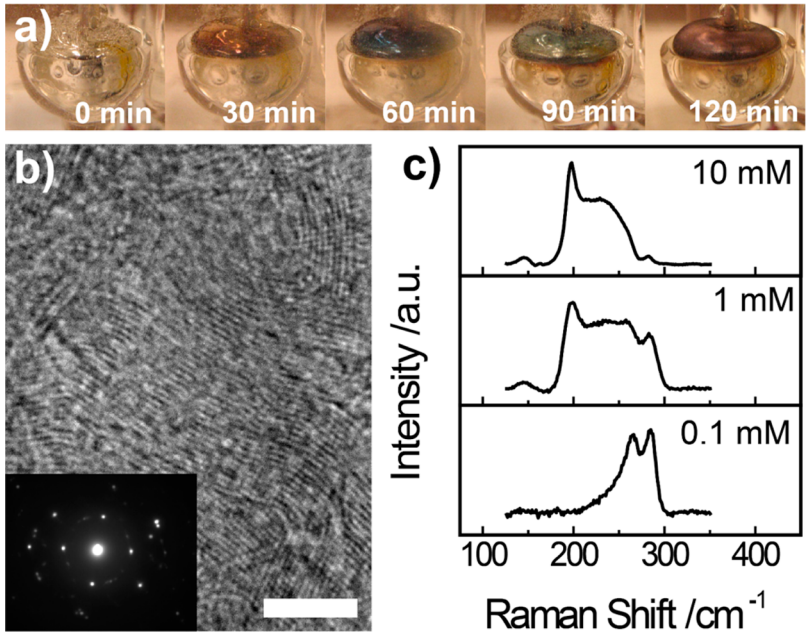

Figure 7. (a) Optical images of a Ga(l) pool electrode immersed in an aqueous solution containing 0.1 M NaOH, 0.1 M Na_2SO_4, and 0.001 M As_2O_3 at 90 °C while biased at −1.58 V for 0, 30, 60, 90, and 120 min. (b) HR-TEM image of GaAs prepared at a Ga(l) pool electrode Scale bar = 5 nm. Inset: SAED pattern for the same sample in (a). (c) Raman spectra for films deposited at Ga(l) pool electrodes immersed in an aqueous solution containing 0.1 M NaOH and 0.1 M Na_2SO_4 at 80 °C with an applied bias of −1.58 V as a function of the formal concentration of As_2O_3. Adapted from ref 34. Copyright 2013 American Chemical Society.

V. PROSPECTS FOR EC-LLS

As shown here, the growth of covalent semiconductor crystals at record low temperatures with just simple benchtop apparatuses is possible. The electrodeposition of fully functional electrical device *components* by ec-LLS is now proven. From this perspective, ec-LLS already occupies a unique place in materials science and is a new step toward non-energy-intensive manufacturing of technologically relevant semiconductors. Still, more work is needed to make ec-LLS a disruptive process at relevant scales. Many simple but practical questions remain regarding the limits of ec-LLS in this context. Can SiO_2 be used as a feedstock for Si ec-LLS? Can ec-LLS be used to make large-area epitaxial thin films? Can photovoltaic-grade heterojunction thin films be made directly through ec-LLS? To what extent can the liquid metal electrode be cleanly separated from the crystals? The answers to these questions will determine the value of ec-LLS to the semiconductor industry.

Irrespective of the answers to these questions, ec-LLS may prove generally valuable for materials chemistry. Microscopic understanding of ec-LLS will not only lead to better resultant materials but should also inform our basic understanding of how crystals (of any type) nucleate and grow. In a separate context, ec-LLS could become useful for the synthesis of compositionally complex inorganic solids. The reactivity of metals dissolved in liquid metal electrodes has been recognized for decades,[59] but mostly as an unwanted complication in polarographic sensing methods. In this way, ec-LLS may be a versatile synthetic method that complements traditional inorganic flux syntheses.[60] Only time will tell what future directions research in ec-LLS may take. This Account is just the beginning of the development of ec-LLS.

■ AUTHOR INFORMATION

Corresponding Author

*E-mail: smald@umich.edu.

Notes

The authors declare no competing financial interest.

Biography

Eli Fahrenkrug graduated with a B.S. in Chemistry from The Evergreen State College in 2011 and is presently a Ph.D. student in the Department of Chemistry at the University of Michigan, working under the direction of Prof. Stephen Maldonado. His research focuses on semiconductor crystallization from liquid metals under electrochemical control.

Stephen Maldonado received his B.S. in Chemistry from the University of Iowa and started graduate research at the University of Texas at Austin in 2001. Following graduation in 2006, he joined the laboratory of Prof. Nathan S. Lewis at the California Institute of Technology. In 2008, he became a faculty member in the Department of Chemistry at the University of Michigan, Ann Arbor. His group works in the area of semiconductor electrochemistry, focusing on the design and electrodeposition of nanostructured semiconductor electrodes.

■ ACKNOWLEDGMENTS

S.M. is the recipient of a Camille Dreyfus Teacher Scholar Award and a Sloan Fellowship. The donors of the American Chemical Society Petroleum Research Fund (51339-DNI5) are acknowledged for support of some of the presented results. The contributions from many undergraduate and graduate student researchers listed as coauthors on our ec-LLS works are duly appreciated and recognized.

DOI: 10.1021/acs.accounts.5b00158
Acc. Chem. Res. 2015, 48, 1881−1890

REFERENCES

(1) Hu, C. *Modern Semiconductor Devices for Integrated Circuits*; Prentice Hall: Upper Saddle River, NJ, 2010.
(2) Razeghi, M.; Rogalski, A. Semiconductor ultraviolet detectors. *J. Appl. Phys.* **1996**, *79*, 7433−7473.
(3) Shah, A.; Torres, P.; Tscharner, R.; Wyrsch, N.; Keppner, H. Photovoltaic technology: The case for thin-film solar cells. *Science* **1999**, *285*, 692−698.
(4) Razykov, T. M.; Ferekides, C. S.; Morel, D.; Stefanakos, E.; Ullal, H. S.; Upadhyaya, H. M. Solar photovoltaic electricity: Current status and future prospects. *Sol. Energy* **2011**, *85*, 1580−1608.
(5) Cowley, A. H.; Jones, R. A. Single-Source III/V Precursors: A New Approach to Gallium Arsenide and Related Semiconductors. *Angew. Chem., Int. Ed. Engl.* **1989**, *28*, 1208−1215.
(6) Tao, C. S.; Jiang, J.; Tao, M. Natural resource limitations to terawatt-scale solar cells. *Sol. Energy Mater.* **2011**, *95*, 3176−3180.
(7) Williams, E. D.; Ayres, R. U.; Heller, M. The 1.7 Kilogram Microchip: Energy and Material Use in the Production of Semiconductor Devices. *Environ. Sci. Technol.* **2002**, *36*, 5504−5510.
(8) Razeghi, M. Compound Semiconductors and Crystal Growth Techniques. In *Fundamentals of Solid State Engineering*; Springer: New York, 2002; pp 349−386.
(9) *Liquid Phase Epitaxy of Electronic, Optical and Optoelectronic Materials*; Capper, P., Mauk, M., Eds.; Wiley: Chichester, U.K., 2007.
(10) Dost, S.; Lent, B. *Single Crystal Growth of Semiconductors from Metallic Solutions*; Elsevier: Amsterdam, 2007.
(11) Bryskiewicz, T. Liquid-Phase Electroepitaxy of Semiconductor Compounds. *Prog. Cryst. Growth Charact.* **1986**, *12*, 29−43.
(12) Law, M.; Goldberger, J.; Yang, P. Semiconductor Nanowires and Nanotubes. *Annu. Rev. Mater. Res.* **2004**, *34*, 83−122.
(13) Lu, W.; Lieber, C. M. Semiconductor nanowires. *J. Phys. D: Appl. Phys.* **2006**, *39*, R387−R406.
(14) Kolasinski, K. W. Catalytic growth of nanowires: Vapor−liquid−solid, vapor−solid−solid, solution−liquid−solid and solid−liquid−solid growth. *Curr. Opin. Solid State Mater. Sci.* **2006**, *10*, 182−191.
(15) Westwater, J.; Gosain, D. P.; Tomiya, S.; Usui, S.; Ruda, H. Growth of silicon nanowires via gold/silane vapor−liquid−solid reaction. *J. Vac. Sci. Technol., B* **1997**, *15*, 554−557.
(16) Wang, F. D.; Dong, A. G.; Sun, J. W.; Tang, R.; Yu, H.; Buhro, W. E. Solution−liquid−solid growth of semiconductor nanowires. *Inorg. Chem.* **2006**, *45*, 7511−7521.
(17) Yang, H.-J.; Yuan, F.-W.; Tuan, H.-Y. Vapor−liquid−solid growth of silicon nanowires using organosilane as precursor. *Chem. Commun.* **2010**, *46*, 6105−6107.
(18) Kim, B. J.; Wen, C. Y.; Tersoff, J.; Reuter, M. C.; Stach, E. A.; Ross, F. M. Growth Pathways in Ultralow Temperature Ge Nucleation from Au. *Nano Lett.* **2012**, *12*, 5867−5872.
(19) McAlpine, M. C.; Ahmad, H.; Wang, D.; Heath, J. R. Highly ordered nanowire arrays on plastic substrates for ultrasensitive flexible chemical sensors. *Nat. Mater.* **2007**, *6*, 379−384.
(20) Renard, V. T.; Jublot, M.; Gergaud, P.; Cherns, P.; Rouchon, D.; Chabli, A.; Jousseaume, V. Catalyst preparation for CMOS-compatible silicon nanowire synthesis. *Nat. Nanotechnol.* **2009**, *4*, 654−657.
(21) Melloch, M. R.; Woodall, J. M.; Harmon, E. S.; Otsuka, N.; Pollak, F. H.; Nolte, D. D.; Feenstra, R. M.; Lutz, M. A. Low-Temperature Grown III−V Materials. *Annu. Rev. Mater. Sci.* **1995**, *25*, 547−600.
(22) Zein El Abedin, S.; Endres, F. Electrodeposition of Metals and Semiconductors in Air- and Water-Stable Ionic Liquids. *ChemPhysChem* **2006**, *7*, 58−61.
(23) Meng, X.; Liu, X.; Zhao, J.; Xin, W.; Li, Y. Semiconductor Electrodeposition from Ionic Liquids. *Prog. Chem.* **2010**, *22*, 277−283.
(24) Munisamy, T.; Bard, A. J. Electrodeposition of Si from organic solvents and studies related to initial stages of Si growth. *Electrochim. Acta* **2010**, *55*, 3797−3803.
(25) Mallet, J.; Molinari, M.; Martineau, F.; Delavoie, F.; Fricoteaux, P.; Troyon, M. Growth of Silicon Nanowires of Controlled Diameters by Electrodeposition in Ionic Liquid at Room Temperature. *Nano Lett.* **2008**, *8*, 3468−3474.
(26) Yang, M. C.; Landau, U.; Angus, J. C. Electrodeposition of GaAs from Aqueous Electrolytes. *J. Electrochem. Soc.* **1992**, *139*, 3480−3488.
(27) Oishi, T.; Watanabe, M.; Koyama, K.; Tanaka, M.; Saegusa, K. Process for Solar Grade Silicon Production by Molten Salt Electrolysis Using Aluminum−Silicon Liquid Alloy. *J. Electrochem. Soc.* **2011**, *158*, E93−E99.
(28) Rao, G. M.; Elwell, D.; Feigelson, R. S. Electrowinning of Silicon from K_2SiF_6−Molten Fluoride Systems. *J. Electrochem. Soc.* **1980**, *127*, 1940−1944.
(29) De Mattei, R. C.; Elwell, D.; Feigelson, R. S. The synthesis of GaAs by molten salt electrolysis. *J. Cryst. Growth* **1978**, *43*, 643−644.
(30) Dalchiele, E.; Cattarin, S.; Musiani, M.; Casellato, U.; Guerriero, P.; Rossetto, G. Electrodeposition of In + As thin film alloys and their conversion to $InAs_xP_{1-x}$ by PH_3 treatment. *J. Electroanal. Chem.* **1996**, *418*, 83−89.
(31) Gregory, B. W.; Stickney, J. L. Electrochemical Atomic Layer Epitaxy (ECALE). *J. Electroanal. Chem.* **1991**, *300*, 543−561.
(32) Gregory, B. W.; Suggs, D. W.; Stickney, J. L. Conditions for the Deposition of CdTe by Electrochemical Atomic Layer Epitaxy. *J. Electrochem. Soc.* **1991**, *138*, 1279−1284.
(33) Carim, A. I.; Collins, S. M.; Foley, J. M.; Maldonado, S. Benchtop Electrochemical Liquid−Liquid−Solid Growth of Nanostructured Crystalline Germanium. *J. Am. Chem. Soc.* **2011**, *133*, 13292−13295.
(34) Fahrenkrug, E.; Gu, J.; Maldonado, S. Electrodeposition of Crystalline GaAs on Liquid Gallium Electrodes in Aqueous Electrolytes. *J. Am. Chem. Soc.* **2013**, *135*, 330−339.
(35) Gu, J.; Fahrenkrug, E.; Maldonado, S. Direct Electrodeposition of Crystalline Silicon at Low Temperatures. *J. Am. Chem. Soc.* **2013**, *135*, 1684−1687.
(36) Fahrenkrug, E.; Biehl, J.; Maldonado, S. Electrochemical Liquid−Liquid−Solid Crystal Growth of Germanium Microwires on Hard and Soft Conductive Substrates at Low Temperature in Aqueous Solution. *Chem. Mater.* **2015**, *27*, 3389−3396.
(37) Fahrenkrug, E.; Gu, J.; Jeon, S.; Veneman, P. A.; Goldman, R. S.; Maldonado, S. Room-Temperature Epitaxial Electrodeposition of Single-Crystalline Germanium Nanowires at the Wafer Scale from an Aqueous Solution. *Nano Lett.* **2014**, *14*, 847−852.
(38) Gu, J.; Collins, S. M.; Carim, A. I.; Hao, X.; Bartlett, B. M.; Maldonado, S. Template-Free Preparation of Crystalline Ge Nanowire Film Electrodes via an Electrochemical Liquid−Liquid−Solid Process in Water at Ambient Pressure and Temperature for Energy Storage. *Nano Lett.* **2012**, *12*, 4617−4623.
(39) Lyon, R. N.; Katz, D. L. *Liquid-Metals Handbook*; U.S. GPO: Washington, DC, 1954.
(40) Assael, M. J.; Armyra, I. J.; Brillo, J.; Stankus, S. V.; Wu, J.; Wakeham, W. A. Reference Data for the Density and Viscosity of Liquid Cadmium, Cobalt, Gallium, Indium, Mercury, Silicon, Thallium, and Zinc. *J. Phys. Chem. Ref. Data* **2012**, *41*, No. 033101.
(41) Grosse, A. A. V. The Relationship between Surface Tension and Energy of Liquid Metals and Their Heat of Vaporization at the Melting Point. *J. Inorg. Nucl. Chem.* **1964**, *26*, 1349−1361.
(42) Keck, P. H.; Broder, J. The Solubility of Silicon and Germanium in Gallium and Indium. *Phys. Rev.* **1953**, *90*, 521−522.
(43) Guminski, C. The Hg−Si System. *J. Phase Equilib.* **2001**, *22*, 682−683.
(44) Guminski, C. The Ge−Hg System. *J. Phase Equilib.* **1999**, *20*, 344−346.
(45) Holze, R. *Electrochemical Thermodynamics and Kinetics*; Landolt-Börnstein: Numerical Data and Functional Relationships in Science and Technology - New Series, Vol. *9A*; Springer: Berlin, 2007; pp 330−441.
(46) Vekilov, P. G. Nucleation. *Cryst. Growth Des.* **2010**, *10*, 5007−5019.
(47) Cho, S. K.; Fan, F.-R. F.; Bard, A. J. Electrodeposition of Crystalline and Photoactive Silicon Directly from Silicon Dioxide Nanoparticles in Molten $CaCl_2$. *Angew. Chem.* **2012**, *124*, 12912−12916.

DOI: 10.1021/acs.accounts.5b00158
Acc. Chem. Res. 2015, 48, 1881−1890

(48) Schmidt, V.; Wittemann, J. V.; Gösele, U. Growth, Thermodynamics, and Electrical Properties of Silicon Nanowires. *Chem. Rev.* **2010**, *110*, 361−388.
(49) Ma, L.; Gu, J.; Fahrenkrug, E.; Maldonado, S. Electrochemical Liquid−Liquid−Solid Deposition of Crystalline Ge Nanowires as a Function of Ga Nanodroplet Size. *J. Electrochem. Soc.* **2014**, *161*, D3044−D3050.
(50) Bottomley, D. J.; Iwami, M.; Uehara, Y.; Ushioda, S. Evidence for liquid indium nanoparticles on Ge(001) at room temperature. *J. Vac. Sci. Technol., B* **1999**, *17*, 12−21.
(51) Mahenderkar, N. K.; Liu, Y.-C.; Koza, J. A.; Switzer, J. A. Electrodeposited Germanium Nanowires. *ACS Nano* **2014**, *8*, 9524−9530.
(52) Penner, R. M. Mesoscopic Metal Particles and Wires by Electrodeposition. *J. Phys. Chem. B* **2002**, *106*, 3339−3353.
(53) Graetz, J.; Ahn, C. C.; Yazami, R.; Fultz, B. Nanocrystalline and Thin Film Germanium Electrodes with High Lithium Capacity and High Rate Capabilities. *J. Electrochem. Soc.* **2004**, *151*, A698−A702.
(54) Rudawski, N. G.; Darby, B. L.; Yates, B. R.; Jones, K. S.; Elliman, R. G.; Volinsky, A. A. Nanostructured Ion Beam-Modified Ge Films for High Capacity Li Ion Battery Anodes. *Appl. Phys. Lett.* **2012**, *100*, No. 083111.
(55) Laforge, B.; Levan-Jodin, L.; Salot, R.; Billard, A. A Study of Germanium as Electrode in Thin-Film Battery. *J. Electrochem. Soc.* **2008**, *155*, A181−A188.
(56) Lee, H.; Kim, M. G.; Choi, C. H.; Sun, Y.-K.; Yoon, C. S.; Cho, J. Surface-Stabilized Amorphous Germanium Nanoparticles for Lithium-Storage Material. *J. Phys. Chem. B* **2005**, *109*, 20719−20723.
(57) Park, M. H.; Kim, K.; Kim, J.; Cho, J. Flexible Dimensional Control of High-Capacity Li-Ion-Battery Anodes: From 0D Hollow to 3D Porous Germanium Nanoparticle Assemblies. *Adv. Mater.* **2010**, *22*, 415−418.
(58) Fahrenkrug, E.; Gu, J.; Maldonado, S. Electrochemically Gated Alloy Formation of Crystalline InAs Thin Films at Room Temperature in Aqueous Electrolytes. *Chem. Mater.* **2014**, *26*, 4535−4543.
(59) Kemula, W.; Kublik, Z.; Galus, Z. Influence of Gold in a Mercury Electrode on Certain Electrode Processes. *Nature* **1959**, *184*, B.A.56−B.A.57.
(60) Kanatzidis, M. G.; Pöttgen, R.; Jeitschko, W. The Metal Flux: A Preparative Tool for the Exploration of Intermetallic Compounds. *Angew. Chem., Int. Ed.* **2005**, *44*, 6996−7023.

DOI: 10.1021/acs.accounts.5b00158
Acc. Chem. Res. 2015, 48, 1881−1890